Geophysical Research Letters

RESEARCH LETTER
10.1029/2025GL119507

Fault Kinematic Controls on the Spatio-Temporal Proximity of the 2023 Mw 7.8-7.7 Türkiye Earthquakes

Wenbin Xu[1,2], Kai Sun[1,2], Qijie Wang[1,2], Guojie Meng[3], Lei Xie[1,2], and Ali Özkan[4,5]

[1]School of Geoscience and Info-Physics, Central South University, Changsha, China, [2]Key Laboratory of Metallogenic Prediction of Nonferrous Metals and Geological Environment Monitoring Ministry of Education, Changsha, China, [3]Key Laboratory of Earthquake Forecasting, China Earthquake Administration, Beijing, China, [4]Institut Terre et Environnement de Strasbourg (ITES), CNRS UMR 7063, Université de Strasbourg, Strasbourg, France, [5]Osmaniye Vocational School, Osmaniye Korkut Ata University, Osmaniye, Türkiye

Abstract The mechanism governing the spatio-temporal proximity of the 2023 Mw 7.8-7.7 Türkiye earthquakes remains enigmatic. Here, we used dense geodetic observations integrated with dual-fault screw dislocation, Euler-vector-constrained block, and strain-rate models to investigate the interseismic kinematics and pre-stress state of the East Anatolian Fault Zone (EAFZ). We showed that the Pazarcık and Çardak segments exhibit slip rates of 6.0–7.5 mm/yr and 2.0–2.5 mm/yr, respectively, reconciling long-standing geodetic-geologic discrepancies in regional slip partitioning. We found ambient pre-stress both promotes rupture cascades on single strands and prevents inter-strand propagation, segmenting ruptures into doublet events. Strain localization and strain-axes rotation provide geodetic evidence for lithospheric heterogeneity control between the Arabian and Anatolian plates over the kinematic behavior and seismic activity of the EAFZ. Our study highlights the seismic risk arising from near-synchronous ruptures of fault systems shaped by lithospheric heterogeneity across crustal and mantle depths.

Plain Language Summary In February 2023, two devastating earthquakes (Mw 7.8 and Mw 7.7) struck Türkiye's East Anatolian Fault Zone, rupturing both its main and secondary branches within hours. To understand why two earthquakes occurred so close in time and space, we studied the fault behavior before the events using satellite measurements. Our analysis reveals that the two fault branches were moving at different speeds between earthquakes, matching long-term geological slip rates. The larger Mw 7.8 earthquake released nearly all the accumulated strain on the main branch, while the smaller Mw 7.7 earthquake released more energy than expected from recent strain buildup, which may reflect biases in historical earthquake records. Our analysis also reveals that stress patterns in the ground helped steer the earthquake ruptures, particularly directing the larger quake toward the Doğanşehir area, while stress heterogeneity along the fault explains why the two sections broke at different times. A major implication from our results is that the slow collision between the Arabian and Anatolian tectonic plates may shape earthquake behavior from depth. Our work highlights the need to better assess risks in complex fault systems where multiple branches can break together, potentially causing even more destructive earthquakes in the future.

Key Points:

- Geodetic-geologic inconsistency in slip partitioning between main and secondary strands of the EAFZ was largely reconciled
- Stress heterogeneity facilitated rupture propagation in individual events while segregating the doublet
- Lithospheric heterogeneity likely governs regional strain partitioning and strain-axis rotation, enabling the Türkiye earthquake doublet

Supporting Information:

Supporting Information may be found in the online version of this article.

Correspondence to:

K. Sun,
kai.sun@csu.edu.cn

Citation:

Xu, W., Sun, K., Wang, Q., Meng, G., Xie, L., & Özkan, A. (2026). Fault kinematic controls on the spatio-temporal proximity of the 2023 Mw 7.8-7.7 Türkiye Earthquakes. *Geophysical Research Letters*, *53*, e2025GL119507. https://doi.org/10.1029/2025GL119507

Received 16 SEP 2025
Accepted 7 MAR 2026

Author Contributions:

Conceptualization: Wenbin Xu
Formal analysis: Wenbin Xu, Kai Sun
Funding acquisition: Wenbin Xu, Qijie Wang, Lei Xie
Investigation: Ali Özkan
Methodology: Wenbin Xu, Guojie Meng, Ali Özkan
Software: Kai Sun
Supervision: Wenbin Xu, Qijie Wang
Validation: Wenbin Xu, Qijie Wang, Guojie Meng
Visualization: Kai Sun
Writing – original draft: Wenbin Xu, Kai Sun

1. Introduction

The seismo-tectonic setting of Türkiye and its surroundings is characterized by complex plate interactions and frequent seismic activities, due to the ongoing convergence of the Eurasian, Arabian, and African plates (Figure 1a). Bounded by the conjugate North Anatolian Fault Zone (NAFZ) and East Anatolian Fault Zone (EAFZ), the Anatolian microplate escapes westward under the push from the Eurasian/Arabian collision in the east and the pull from the Hellenic retreat in the south and west (Figure 1a; e.g., Le Pichon & Kreemer, 2010; McKenzie, 1976). The relative lateral movement in the north is primarily concentrated along the NAFZ (e.g., Armijo et al., 1999; Barbot & Weiss, 2021). In contrast, the lateral escape accommodated in the southeast involves the EAFZ and a series of intra-plate secondary structures, forming an extensive sinistral shear zone (Figure 1b; e.g., Duman & Emre, 2013; Seyitoğlu et al., 2022).

On 6 February 2023, a moment magnitude (Mw) 7.8 earthquake (hereinafter referred to as the Pazarcık earthquake) ruptured the main (southern) strand of the EAFZ, extending from Çelikhan to the Hatay Triple Junction (Figure 1c). Approximately 9 hr later, a Mw 7.7 earthquake (hereinafter the Elbistan earthquake) occurred 95 km to the north, rupturing the Savrun-Çardak segment of the secondary (northern) strand and the adjacent Doğanşehir

Writing – review & editing: Wenbin Xu, Kai Sun, Qijie Wang, Guojie Meng, Lei Xie, Ali Özkan

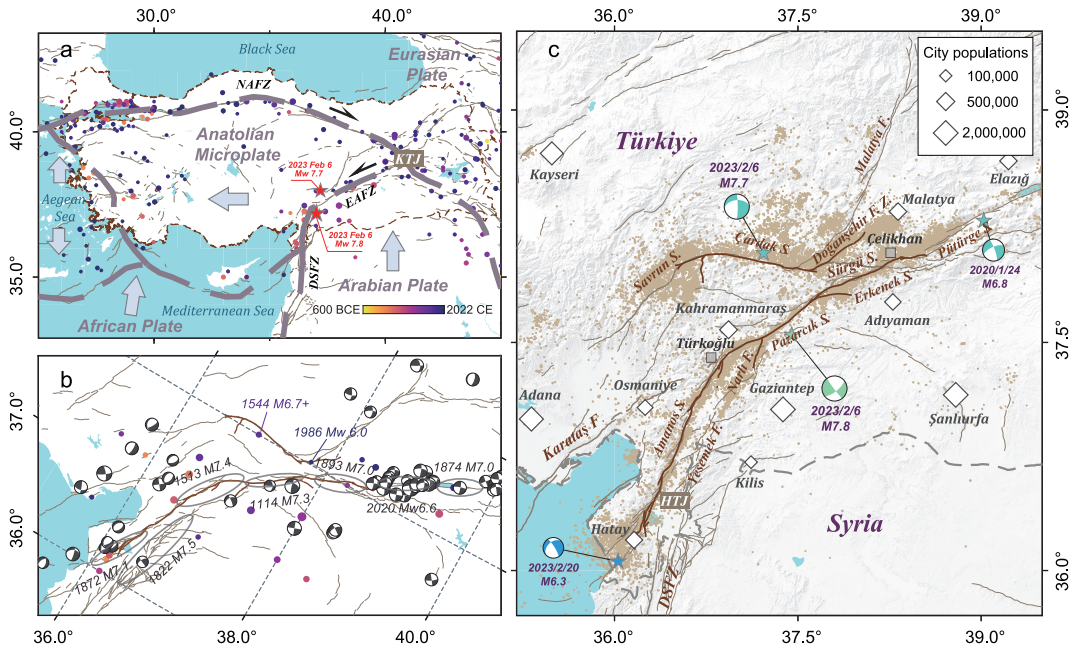

Figure 1. Seismo-Tectonic setting of the 2023 Türkiye earthquake doublet. (a) Plate dynamics and strong earthquakes in the eastern Mediterranean. Colored dots show strong earthquakes (M ≥ 6.0) from 600 BCE to 2022 CE (Tan, 2021; Tan et al., 2008). DSFZ, Dead Sea Fault Zone; KTJ, Karlıova Triple Junction. (b) Earthquakes in Eastern Anatolia. The brown solid lines show the rupture traces of the earthquake doublet (Reitman et al., 2023). Beach balls represent earthquakes with Mw ≥ 4.5 from 1976 to 2023 (GCMT; https://www.globalcmt.org/). Ellipses show the historical rupture zones (Carena et al., 2023). Gray solid lines show active fault traces (Zelenin et al., 2022). (c) Fault segmentation, aftershock distribution, and city populations in the source area. Yellow dots indicate aftershocks with Mw > 1.5 four months after the mainshock (Lomax, 2023). HTJ: Hatay Triple Junction.

fault zone (Figure 1c). Despite known seismic potential in SE Türkiye, the occurrence of two major earthquakes in such spatio-temporal proximity was unexpected, causing over 60,000 fatalities and displacing millions (Carena et al., 2023; Nalbant et al., 2002; STL, 2024).

The temporal proximity of the earthquake doublet is attributed to Coulomb stress loading from the Pazarcık earthquake, which triggered the Elbistan earthquake decades early, following millennia of strain accumulation (e.g., J. Chen et al., 2024; Jia et al., 2023). Fault slip rates are crucial for quantifying interseismic strain accumulation; however, significant discrepancies persist among studies regarding slip partitioning between the two strands of the EAFZ (e.g., Duman & Emre, 2013; He et al., 2023; Vavra et al., 2025). Following the earthquake doublet, two different studies that investigated slip partitioning between the Pazarcık and Çardak segments showed contrasting results: one derived slip rates of 4.6 ± 0.7 mm/yr and 3.9 ± 0.7 mm/yr (He et al., 2023), while the other derived 8.0 ± 0.5 mm/yr and 4.7 ± 0.3 mm/yr (Vavra et al., 2025). Accordingly, He et al. (2023) attributed the temporal clustering of the doublet to synchronized ruptures driven by long-term stress interactions between the two strands. However, their inferred interseismic slip deficit fails to account for the large coseismic slip. In contrast, Vavra et al. (2025) suggested that the slip deficit of the Pazarcık earthquake was marginally smaller than its coseismic slip, potentially due to cascading ruptures facilitating the release of residual stress, whereas the Elbistan earthquake exhibited moment balance. Notably, both geodetic estimates deviate from the geological slip rates of 6.5–7.0 mm/yr and ~2.5 mm/yr for these segments (Duman & Emre, 2013). The inconsistency in fault slip rates significantly impedes our understanding of the interseismic kinematics along the EAFZ and the energy build-up process of this earthquake doublet.

The spatial proximity of this earthquake doublet arises from the coordinated interplay between fault strike variations and ambient pre-stress heterogeneity (K. Chen et al., 2024). Intriguingly, the Sürgü segment, which structurally links the ruptured segments of the earthquake doublet and experienced significant Coulomb stress loading from the Pazarcık earthquake, remained seismically silent during the event (Jia et al., 2023). The underlying controls on inhibiting cascading rupture between two strands during this earthquake doublet, and

whether they could potentially generate catastrophic earthquakes through throughgoing rupture, remain unresolved.

Here, we address these concerns by investigating the interseismic behavior of the EAFZ and its connection to the earthquake doublet using geodetic data. First, we derive slip rates and coupling distribution along both strands using dual-fault screw dislocation and Euler-vector-constrained block models. Next, we analyze the correlation between cumulative slip deficit and coseismic slip. We then explore how pre-stress heterogeneity controls cascading rupture across segments. Finally, we synthesize these results into a seismogenic framework for the doublet and discuss implications for hazard assessment in complex tectonic zones.

2. Data and Methods

2.1. Reference Frame Unification of Geodetic Data

The dense GNSS network used in this study integrates three data sets: the velocity fields published by Ergintav et al. (2023) and Kurt et al. (2023), along with additional campaign data from Özkan et al. (2023) that extends the geodetic network originally established by Mahmoud et al. (2013). All observations were collected before the 2020 Mw 6.8 Elazığ earthquake, representing steady-state interseismic deformation. The velocity fields from the other two studies are referenced to Kurt et al. (2023) by solving rotation parameters for velocity misfits at common stations using a weighted least squares approach (Figure S1 in Supporting Information S1). The root-mean-square (RMS) values of the post-transformation misfits are less than 1 mm/yr (Table S1 in Supporting Information S1). The InSAR dataset used in this study is sourced from Weiss et al. (2020), spanning 2014 to 2019. Line-of-sight (LOS) velocities within each track are tied to the GNSS reference frame through residual plane fitting.

2.2. Screw Dislocation Modeling and Inversion

Fault slip rates can be estimated by constructing fault-perpendicular profiles using elastic half-space screw dislocation models, assuming the modeled faults account for all surface deformation (Savage & Burford, 1973; Weertman & Weertman, 1964). We integrate two screw dislocations to interpret surface deformation caused by the two strands of the EAFZ. These dislocations independently resolve the distance to and deformation zone of each strand, thereby accounting for spatial offsets and strike variations between the strands. The surface deformation in LOS is formulated as:

$$V_{\mathrm{los}} = aV_{\mathrm{par}} + bV'_{\mathrm{par}} = a\frac{S}{\pi}\tan^{-1}\left(\frac{x-\xi}{D_L}\right) + b\frac{S'}{\pi}\tan^{-1}\left(\frac{x'-\xi'}{D'_L}\right) + c \tag{1}$$

Where V_{par} and V'_{par} denote the fault-parallel velocities of the main and secondary strands, respectively. S and D_L represent the slip rate and locking depth, while x denotes the perpendicular distance from the observation to the main strand. ξ is the deformation offset induced by the non-vertical fault geometry, expressed as $\xi = D_L/\tan(\alpha)$, where α represents the dip angle. Symbols with superscripts denote parameters associated with the secondary strand. c is a constant. a and b are coefficient matrices for InSAR geometric and fault-parallel component projections and deformation zone constraint:

$$\begin{cases} a = \sin(\theta)(\cos(\gamma)\sin(\alpha) - \sin(\gamma)\cos(\alpha)) \\ b = p\sin(\theta)(\cos(\gamma)\sin(\alpha') - \sin(\gamma)\cos(\alpha')) \end{cases} \tag{2}$$

where θ and γ are the incidence and heading angles. α and α' are strikes of the main and secondary strands. $p = 1$ if the observation lies within the secondary strand's cross-section; otherwise $p = 0$ (Figure S2 in Supporting Information S1).

We constructed two profiles: one spanning the Pazarcık and Çardak segments, and another crossing the Pütürge and Malatya segments (Figure 2a). The locking depths and fault dips are a priori constrained to avoid biases in slip-rate estimates arising from their high sensitivity to near-fault data quality (See Text S1 in Supporting Information S1). We adopted a Bayesian approach to perform nonlinear optimization estimation for the modeled

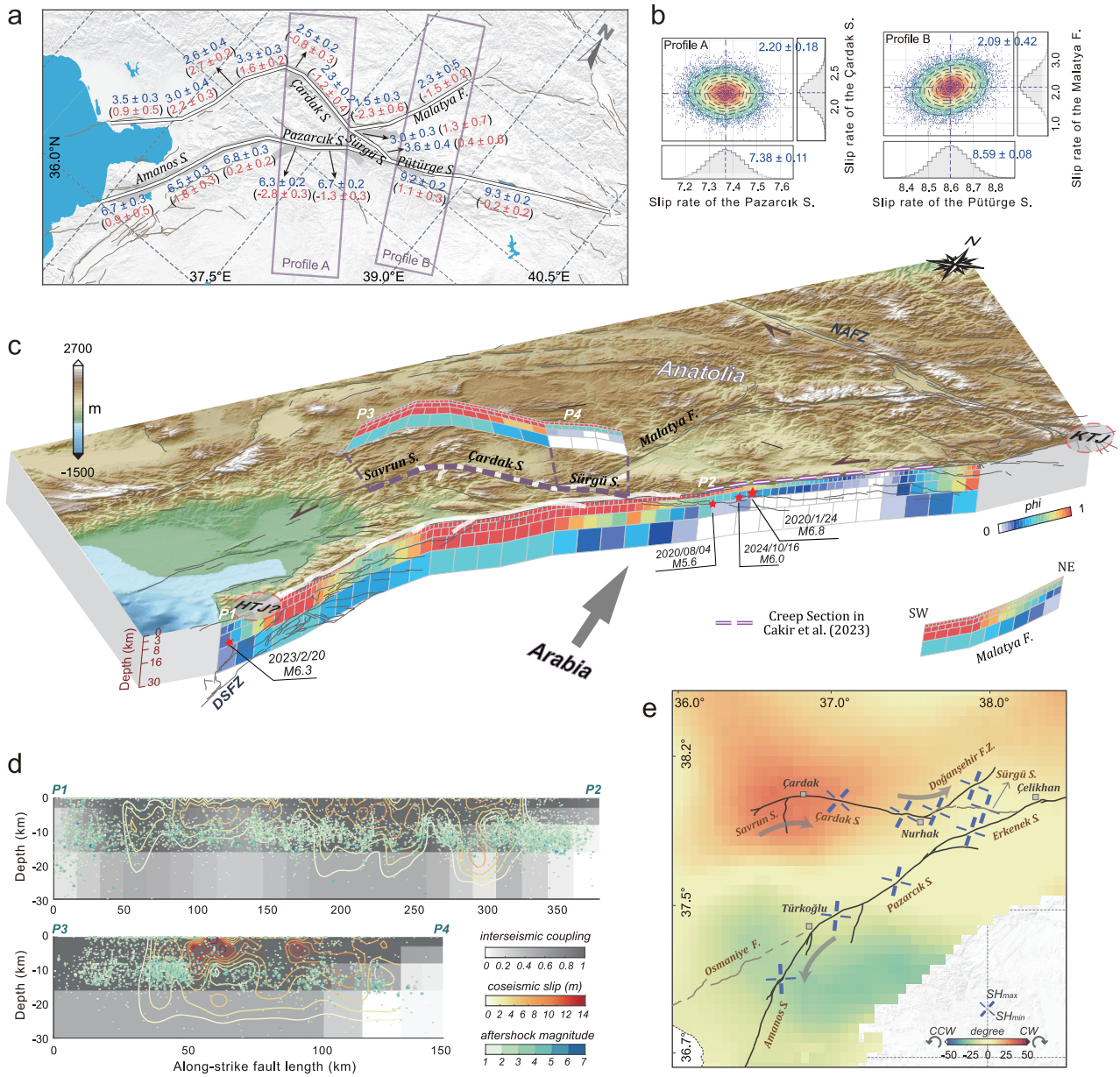

Figure 2. Interseismic kinematics and pre-stress orientations along the EAFZ. (a) Slip rates derived from block modeling. Blue and red values represent fault-parallel and fault-normal slip rates, with positive values indicating sinistral and extensional motion, respectively. Euler vectors for each block relative to the North Arabian Block are listed in Table S2 of Supporting Information S1. (b) Slip rates derived from screw dislocation models. (c) Interseismic coupling along the EAFZ. (d) Superimposed display of inter-seismic coupling, co-seismic slip, and aftershocks. (e) Pre-stress orientations derived from geodetic strain-rate tensors. The base map displays strain rotation angles relative to the reference orientation along the Pazarcık segment. CCW, counterclockwise; CW, clockwise.

kinematic parameters (Foreman-Mackey et al., 2013). A priori ranges for fault slip-rates are set to 0–20 mm/yr. The maximum a posteriori solution and uncertainty of the parameters are estimated after 10, 000, 000 iterations.

2.3. Block Modeling and Inversion

In northern SE Türkiye, block boundaries are clearly delineated by the EAFZ and Malatya fault due to their well-defined structural traces and concentrated seismicity. The southern sector, however, contains scattered secondary structures complicating boundary identification (Figure 1c). We therefore applied Euler-vector clustering, a data-driven strategy applied to the microplate (e.g., Savage, 2018) and subblock (e.g., Xu & Stamps, 2019) geometry

determination, to construct the regional block model (Qu et al., 2022; See Text S2 in Supporting Information S1). The formed cluster boundaries encompassed the rupture traces of the doublet, dividing SE Türkiye into four tectonic blocks (Figures S3 and S4 in Supporting Information S1).

We estimated kinematic parameters of the block-bounding faults using the Tdefnode package (McCaffrey et al., 2007). To account for decreasing model resolution with depth, we divided the fault plane into four layers and progressively increased the patch size as depth increases. Slip rates and coupling coefficients were inverted using grid search and simulated annealing algorithms, with the optimal solution determined by minimizing the reduced chi-square statistic.

2.4. Pre-Stress Orientation Estimation

For tectonic zones lacking sufficient background seismicity, such as the secondary strand of the EAFZ, using geodetic strain-rate tensors to infer stress orientations serves as a viable alternative (K. Chen et al., 2024). We calculated the principal strain rates across the EAFZ and its surroundings using the GNSS velocity field, following the method of Shen et al. (2015). The continuous strain-rate tensor was inverted in a weighted least squares framework by constructing a partial derivative design matrix. We estimated mean stress orientations across nine fault segments spanning the main rupture zones of the earthquake doublet, to analyze correlations between pre-stress conditions and coseismic rupture propagation (Figure S5 in Supporting Information S1). Furthermore, using the stress orientation along the Pazarcık segment as a proxy for plate-boundary stresses, we quantified regional rotation angles relative to the background stress field to identify potential local stress heterogeneities.

3. Results

3.1. Fault Slip Rates, Coupling Distribution, and Strain Rate Field Along the EAFZ

The screw dislocation model determined slip rates of 8.59 ± 0.08 mm/yr and 7.38 ± 0.11 mm/yr for the Pütürge and Pazarcık segments of the main strand of the EAFZ, respectively, and 2.20 ± 0.18 mm/yr for the Çardak segment of the secondary strand (Figure 2b; See Figure S6 in Supporting Information S1 for fitting details). Similarly, the block model estimated slip rates of 9.2 ± 0.2 mm/yr and 6.3 ± 0.2–6.7 ± 0.2 mm/yr for the Pütürge and Pazarcık segments, respectively, and 2.3 ± 0.2–2.5 ± 0.2 mm/yr for the Çardak segment (Figure 2a; See Figures S7–S10 in Supporting Information S1 for fitting details). The slip rates of the Pütürge segment derived from both models are consistent with previous geodetic and geologic estimates of 8–12 mm/yr (e.g., Herece, 2008; Vavra et al., 2025; Walters et al., 2014). However, our results for the Pazarcık and Çardak segments show notable discrepancies with prior geodetic studies, that is, the slip rate of the Çardak segment is neither negligible as suggested by single-fault models (e.g., Aktuğ et al., 2016; Özkan et al., 2023) nor comparable to that of the Pazarcık segment as proposed in the dual-fault model (He et al., 2023). Instead, our results agree better with geologic estimates of 6.5–7.0 mm/yr for the Pazarcık segment and ∼2.5 mm/yr for the Çardak segment (Duman & Emre, 2013). The slip rate of 7.38 ± 0.11 mm/yr determined by the screw-dislocation model for the Pazarcık segment is slightly higher than geological estimates, likely due to unmodeled secondary structures (e.g., the Engizek fault) between the Pazarcık and Çardak segments (Duman & Emre, 2013).

Our block model further revealed a 3.0 ± 0.3–3.6 ± 0.4 mm/yr slip rate for the Sürgü segment, consistent with the Holocene rate of ∼3 mm/yr inferred from drainage network offsets (Figure 2a; Duman & Emre, 2013). Both the screw dislocation (2.09 ± 0.42 mm/yr) and block (1.5 ± 0.3–2.3 ± 0.5 mm/yr) models produced consistent estimates for the Malatya fault, matching chronological surveys and recent seismicity (Figures 2a and 2b; e.g., Sançar et al., 2020). The block model also resolved fault-normal slip rates along the EAFZ (Figure 2a). The Pazarcık segment shows ∼1–3 mm/yr of shortening, while other rupture segments on the main strand are dominated by extension, peaking at 1.8 ± 0.3 mm/yr on the northern Amanos segment. Along the secondary strand, the Çardak segment accommodates 0.8 ± 0.3–1.2 ± 0.4 mm/yr of shortening, whereas all other segments show extensional motion. The western Sürgü segment shows normal faulting motion, consistent with field observations (Balkaya et al., 2023).

A prominent ∼130 km creeping section was identified along the northern main EAFZ, consistent with previous InSAR observations (Figure 2c; Bletery et al., 2020; Cakir et al., 2023). Locking depth increased southwestward, reaching ∼16 km along the central main strand, consistent with the 95% seismicity cutoff (Vavra et al., 2025).

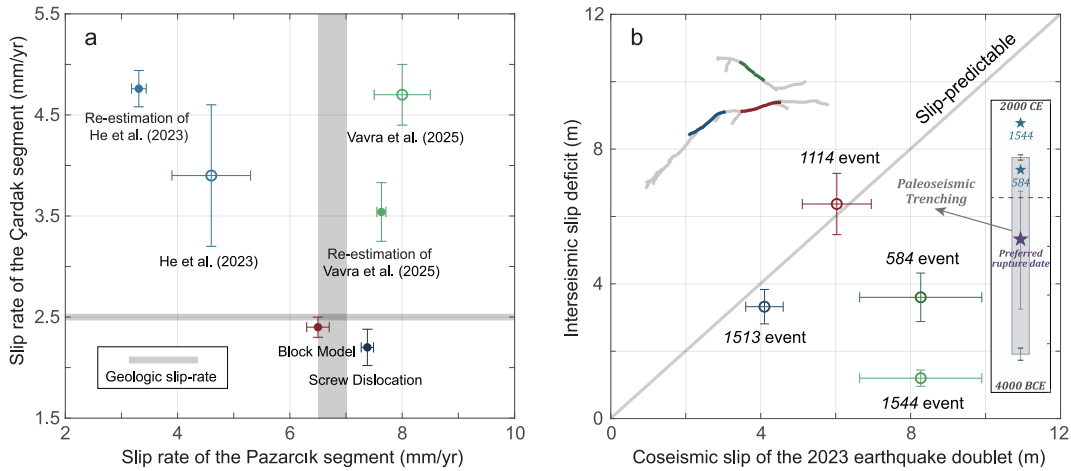

Figure 3. Slip partitioning between the Pazarcık and Çardak segments and slip-predictability of the Türkiye doublet. (a) Slip rates from recent geodetic studies and this study. Geologic slip rates are from Duman and Emre (2013). (b) Comparison of coseismic slip during the earthquake doublet with the slip deficit accumulated over the preceding interseismic period. The parameter values are listed in Table S4 of Supporting Information S1. The gray, red, blue, and green curves represent the rupture traces of the 2023 doublet, the 1114 event, the 1513 event, and the 1544/584 events, respectively (Carena et al., 2023; Reitman et al., 2023).

Notably, the northern Amanos segment exhibited reduced coupling compared to its edges, consistent with the location of maximum normal slip predicted by block model (Figure 2a). The secondary strand displayed deep locking on the Çardak-Savrun segment but weak coupling on the Sürgü segment. Overlay of coseismic slip and interseismic coupling on the seismogenic fault plane showed their first-order spatial correlation (Figure 2d; See Text S3 and Figures S11–S15 in Supporting Information S1 for coseismic inversion details).

Strain-rate field analysis indicated remarkable consistency along the central segment of the main strand of the EAFZ (Figure 2e). After bifurcating into two strands with ∼30° strike separation near Çelikhan, the EAFZ maintained consistent principal strain-rate orientations along both the Erkenek segment of the main strand and the Sürgü segment of the secondary strand. However, southwestward along the main strand, the principal strain-axes underwent a ∼20.6° counterclockwise rotation at the junction between the Pazarcık and Amanos segments. Moving westward along the secondary strand, the strain-axes rotated ∼27.8° clockwise near the middle of the Çardak segment, reaching ∼32° at its linkage with the Savrun segment. The locations of significant strain-axes rotation coincided with structural bends on the main and secondary strands, both of which ruptured during the earthquake doublet. Notably, while the Elbistan earthquake overcame the Nurhak bend to cascade into the Çardak segment and Doğanşehir fault zone, no strain-axes rotation was observed there. These results reveal pronounced spatial heterogeneity in the pre-stress state both between and along the two strands of the EAFZ, despite their close spatial proximity.

4. Discussion

4.1. Inter-Strand Slip Partitioning and Earthquake Recurrence Behavior of the EAFZ

To resolve inconsistencies in slip partitioning estimates between strands of the EAFZ, we evaluated differences in modeling strategies across different geodetic studies (see Text S4, Table S3 and Figures S16–S18 in Supporting Information S1 for details). Our analysis highlights the critical importance of incorporating secondary faults into the model and optimizing the screw dislocation profile length (Figure S18 in Supporting Information S1). Building on insights from these studies, our block and screw-dislocation models provided robust estimates of inter-strand slip partitioning across the EAFZ, achieving high congruence with historical seismicity and geological surveys (Figure 3a).

Comparing interseismic slip deficits with coseismic slip characterizes strain accumulation-release behavior, defining slip-predictability that physically constrains earthquake magnitude prediction (Shimazaki & Nakata, 1980). The historical rupture segments on the EAFZ's main strand have been well identified by recent

multidisciplinary synthesis (Carena et al., 2023). However, the most recent rupture of the secondary strand remains debated. It is widely attributed to either the 1544 M6.7+ earthquake (e.g., Duman & Emre, 2013; Karabulut et al., 2023; Stucchi et al., 2024) or the 584 M7+ event (e.g., Billi et al., 2024; Vavra et al., 2025). Both dates are solely evidenced by historical records of town damage, with no independent geological validation (Ambraseys, 1975; Guidoboni et al., 1994).

For the Pazarcık earthquake, our analysis revealed that the accumulated interseismic strain on the rupture segments of the 1114 and 1513 events approximates the coseismic slip release during the 2023 event, consistent with slip-predictable behavior. In contrast, the slip deficit accumulated on the Çardak segment since its last rupture (either the 1544 or 584 event) is significantly lower than the coseismic slip of the Elbistan earthquake (Figure 3b). Assuming 584 as the most recent rupture date, the discrepancy amounts to 4.67 ± 2.35 m, which cannot be explained by residual stress release and seismic Coulomb stress loading (See Text S5 in Supporting Information S1).

Thus, a longer interseismic period appears necessary for the Çardak segment to produce such large coseismic slip. Paleoseismic trenching indicates the last surface-rupturing event occurred between 3,215 ± 125 BCE and 825 ± 55 CE (Balkaya et al., 2023). By analyzing the slip rate and background stress perturbations, we constrained the timing of the last rupture to 837 BCE, which closely matches the median trench-derived age of 1195 BCE (Figure 3b). These results suggest that the last complete rupture of the Çardak segment likely predates 584 CE. To figure it out, comprehensive paleoseismic investigations are imperative. Moreover, any analysis dependent on isolated documented records, whether for earthquake dating or magnitude inference, requires careful consideration.

4.2. Control of Pre-Stress State on Rupture Propagation in the Earthquake Doublet

Large earthquakes require both long-term strain accumulation on faults and conditions enabling sustained rupture propagation. For the 2023 doublet, their extensive ruptures were driven by dynamic stress interactions between successive sub-events, geometrically favorable fault structures, and ambient pre-stress heterogeneity (e.g., K. Chen et al., 2024; Jia et al., 2023; Ren et al., 2024). At the Türkoğlu bend of the EAFZ, we observed a strain-rate rotation of ∼20.6°, which matches the ∼20° stress rotation inferred from historical focal mechanisms (K. Chen et al., 2024). This consistency reconfirms that the geodetic strain-rate field can serve as a reliable alternative for stress orientation along the EAFZ.

As proposed by K. Chen et al. (2024), the stress rotation at the Türkoğlu bend adjusted the Amanos segment into a failure-favorable orientation, thereby sustaining the rupture propagation of the Pazarcık event along the main strand. Similarly, the ∼27.8° clockwise rotation near Çardak explains how the secondary strand could generate the large-stress-drop Elbistan event, despite its ∼40° strike deviation from the plate boundary (Figure 2e). The Sürgü segment remained seismically silent despite stress loading from the Pazarcık earthquake, attributable to its low degree of coupling (Figures 2c and 2d). Alternatively, the rupture propagated to the stress-shielded Doğanşehir fault zone (Jia et al., 2023). We find that the regional stress rotation does not maintain the entire Çardak-Sürgü structure in an optimally oriented configuration (Figure 2e). From the central Çardak segment to the Sürgü segment, the angle between the maximum compressive stress and fault strike progressively increases, showing enhanced consistency with the plate-boundary stress but deviating from rupture-favorable orientations. In contrast, the Doğanşehir fault zone not only aligns with the background stress but also parallels the main strand of the EAFZ, implying similarly high instability as observed along the Erkenek and Pazarcık segments (Figure 2e; K. Chen et al., 2024). Therefore, as dynamic weakening drove the Elbistan earthquake rupture through the Nurhak bend, the favorable orientation of the Doğanşehir fault zone to the ambient stress field further facilitated sustained rupture propagation.

Paleoseismic investigations on the Çardak and Sürgü segments revealed distinct rupture chronologies, attributable to the barrier effect of an intervening step-over zone (Balkaya et al., 2023). However, this structural obstacle was successfully overcome before the rupture reached the Nurhak bend during the Elbistan event. We therefore propose that the observed temporal discrepancy in rupture timing between the Çardak and Sürgü segments is intrinsically controlled by stress field heterogeneity, which induces distinct rupture segmentation patterns. The persistent rupture asynchrony may place the two segments at different stages of seismic cycles. For instance, during the 2023 Elbistan earthquake, the Sürgü segment remains in a postseismic recovery phase following the 1986 Mw6.0 and Mw5.8 earthquake doublet (Balkaya et al., 2023).

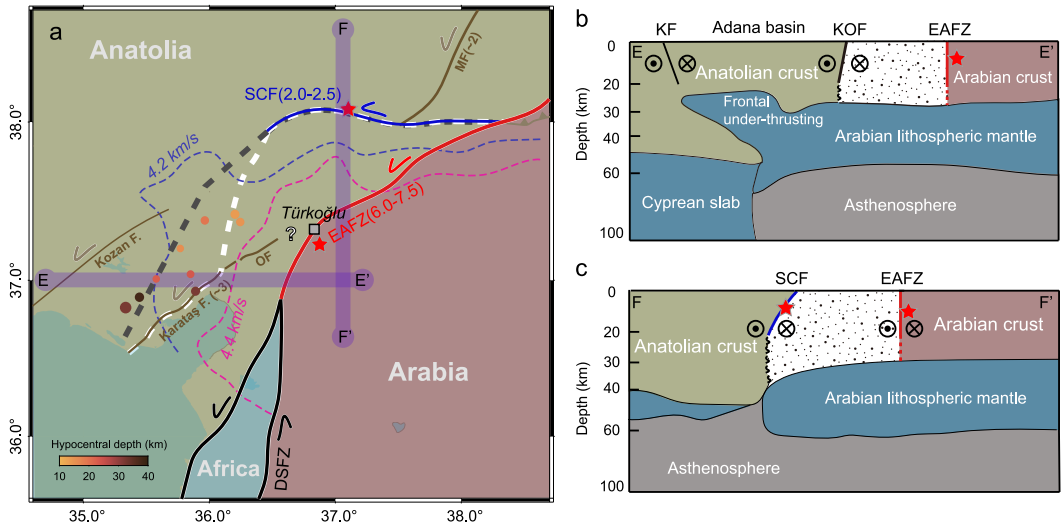

Figure 4. Plate interactions in the Anatolia-Arabia-Africa Junction. (a) Slip partitioning and kinematic boundaries; Lithosphere structures along sections (b) EE' and (c) FF' (Delph et al., 2024). The white dashed line denotes the secondary tectonic boundary identified via geodetic clustering, whereas the dark gray dashed line represents the plate boundaries projected by Delph et al. (2024) for 3 Myr in the future. The pink and blue dashed lines represent the 4.4 and 4.2 km/s shear-wave velocity contours at 40 km depth, respectively (Delph et al., 2017). The earthquake catalog for the Adana basin subsurface is from Ergin et al. (2004). SCF, Sürgü-Çardak Fault; MF, Malatya Fault; OF, Osmaniye Fault; KF, Kozan Fault; KOF, Karataş-Osmaniye Fault.

4.3. Tectonic and Seismic Hazard Implications for SE Türkiye

An unresolved question in regional tectonics is whether a triple junction exists near Türkoğlu (e.g., Duman & Emre, 2013; Özkan et al., 2023; Yönlü et al., 2017). Some studies proposed that the EAFZ merges with the DSFZ here, then propagates southwestward through the Amanos Mountains and connects with the Karataş-Osmaniye fault. Recent geodetic evidence from a GNSS-constrained block model indicates sinistral motion of 3.3–4.5 mm/yr along the southwest-extending structures (Özkan et al., 2023). We adopt a strain-rate differencing strategy to further investigate the active structures overlooked by our block model. Our analysis reveals pronounced strain residuals localized around the Osmaniye fault, indicating its activity, yet with no spatial continuity to the EAFZ (Figure S19 in Supporting Information S1). Furthermore, given the absence of significant aftershock clusters triggered by the Pazarcık earthquake west of Türkoğlu, the existence of a stable triple junction appears less probable (Figure 1c).

In contrast, seismic tomography and crustal thickness across the Arabian-Anatolian convergent margin reveal lithospheric mantle indentation into the rheologically weaker crust, thereby defining a broad deformation zone (Delph et al., 2024; Karabulut et al., 2019; Figure 4a). The upper crust of the Arabian and Anatolian plates converges along the main strand of the EAFZ, consistent with the primary tectonic boundary identified through geodetic cluster analysis (Figure S4b in Supporting Information S1). At depth, the underthrusting of the strong Arabian lithospheric mantle into the Anatolian plate extends northward to the Sürgü-Çardak segment and westward to the central Adana Basin (Delph et al., 2024; Figure 4b). Secondary deformation boundaries are consistent with the shear-wave velocity gradient and the Arabian mantle front boundary to first-order approximation, except for the eastward offset of the central Adana basin to the Karataş fault (Figure 4a). This offset is attributed to a higher elastic strain accumulation rate on the Karataş fault than in the Adana basin, with the former characterized by shallower hypocenters and more frequent, intense seismicity (Figures 1b and 4a; Ergin et al., 2004). Furthermore, our findings revealed spatial correlations between stress field heterogeneities and the crust-mantle architecture across the plate boundary (Figures 2a, 2e and 4). Under Arabian-Anatolian crustal collision, the stress field exhibits uniformity along the EAFZ's main strand and the intraplate Doğanşehir fault zone. Conversely, the Sürgü-Çardak segment exhibits a clockwise rotation of stress orientation relative to the background field, spatially coincident with the northward indentation of the deep, strong Arabian mantle.

Collectively, the spatial proximity of these two devastating earthquakes may primarily be attributed to rheological contrasts between the Arabian and Anatolian plates, which govern strain localization under shared tectonic forcing. Concurrently, stress heterogeneity induces spatio-temporal rupture segmentation, naturally forming barriers that inhibit cascading rupture between the two strands of the EAFZ. Under these conditions, accumulated strain on both strands is released through static stress triggering, generating an earthquake doublet. The 2023 Türkiye doublet exemplifies such a systematic rupture in a supercycle, underscoring the necessity of comprehensive investigations into secondary fault activity.

Conflict of Interest

The authors declare no conflicts of interest relevant to this study.

Availability Statement

The integrated interseismic GNSS velocity field and coseismic deformation fields can be downloaded from the Zenodo repository (Sun, 2025). Other data used in this study have been published and made available by the authors cited in the references list: the active fault database (Zelenin et al., 2022, https://doi.org/10.5194/essd-14-4489-2022 [Dataset]), the instrumental earthquake catalog for Türkiye (Tan, 2021, https://doi.org/10.5194/nhess-21-2059-2021 [Dataset]), the rupture traces of earthquakes in the Türkiye-Syria border region from 1000 CE to the present (Carena et al., 2023, https://doi.org/10.1029/2023TC007890 [Dataset]), and the interseismic InSAR velocity field (Weiss et al., 2020, https://doi.org/10.1029/2020GL087376 [Dataset]). The coseismic slip inversion code is archived on Zenodo (Jin & Fialko, 2021). Figures are produced using the Generic Mapping Tools 6.4.0 software (Wessel et al., 2019).

Acknowledgments

The authors thank the editor Fabio Capitanio, Dr. Zhangfeng Ma, and an anonymous reviewer for their thoughtful comments and suggestions, which have significantly improved the manuscript. This work was supported by National Natural Science Foundation of China (42388102, 42304037), Natural Science Foundation of Hunan Province (2024JJ3031), Science and Technology Innovation Program of Fujian Province (2021Y3001), Science and Technology Innovation Program of Hunan Province (2023SK2012), and the Fundamental Research Funds for the Central Universities of Central South University (2024ZZTS0368). The authors warmly thank Prof. Rob McCaffrey for his guidance on Tdefnode software and Dr. Zeyu Jin for the help with coseismic slip inversion. The authors thank Dr. Guoguang Wei and Prof. Chang Liu for their insightful discussions.

References

Aktuğ, B., Ozener, H., Dogru, A., Sabuncu, A., Turgut, B., Halicioglu, K., et al. (2016). Slip rates and seismic potential on the East Anatolian Fault System using an improved GPS velocity field. *Journal of Geodynamics*, *94–95*, 1–12. https://doi.org/10.1016/j.jog.2016.01.001

Ambraseys, N. N. (1975). Studies in historical seismicity and tectonics. In *Geodynamics today: A review of the Earth's dynamic processes* (pp. 7–16). Royal Society.

Armijo, R., Meyer, B., Hubert, A., & Barka, A. (1999). Westward propagation of the North Anatolian fault into the northern Aegean: Timing and kinematics. *Geology*, *27*(3), 267. https://doi.org/10.1130/0091-7613(1999)027<0267:WPOTNA>2.3.CO;2

Balkaya, M., Akyüz, H. S., & Özden, S. (2023). Paleoseismology of the Sürgü and Çardak faults-splays of the Eastern Anatolian fault Zone, Türkiye. *Turkish Journal of Earth Sciences*, *32*(3), 402–420. https://doi.org/10.55730/1300-0985.1851

Barbot, S., & Weiss, J. R. (2021). Connecting subduction, extension and shear localization across the Aegean Sea and Anatolia. *Geophysical Journal International*, *226*(1), 422–445. https://doi.org/10.1093/gji/ggab078

Billi, A., Corbi, F., Cuffaro, M., Orecchio, B., Palano, M., Presti, D., & Totaro, C. (2024). Seismic slip channeling along the East Anatolian Fault illuminates long-term supercycle behavior. *Nature Communications*, *15*(1), 8921. https://doi.org/10.1038/s41467-024-53234-0

Bletery, Q., Cavalié, O., Nocquet, J., & Ragon, T. (2020). Distribution of interseismic coupling along the north and East Anatolian faults inferred from InSAR and GPS data. *Geophysical Research Letters*, *47*(16), e2020GL087775. https://doi.org/10.1029/2020GL087775

Cakir, Z., Doğan, U., Akoğlu, A. M., Ergintav, S., Özarpacı, S., Özdemir, A., et al. (2023). Arrest of the Mw 6.8 January 24, 2020 Elaziğ (Turkey) earthquake by shallow fault creep. *Earth and Planetary Science Letters*, *608*, 118085. https://doi.org/10.1016/j.epsl.2023.118085

Carena, S., Friedrich, A. M., Verdecchia, A., Kahle, B., Rieger, S., & Kübler, S. (2023). Identification of source faults of large earthquakes in the Turkey-Syria border Region between 1000 CE and the present, and their relevance for the 2023 Mw 7.8 pazarcık earthquake. *Tectonics*, *42*(12), e2023TC007890. https://doi.org/10.1029/2023TC007890

Chen, J., Liu, C., Dal Zilio, L., Cao, J., Wang, H., Yang, G., et al. (2024). Decoding stress patterns of the 2023 Türkiye-Syria earthquake doublet. *Journal of Geophysical Research: Solid Earth*, *129*(10), e2024JB029213. https://doi.org/10.1029/2024JB029213

Chen, K., Wei, G., Milliner, C., Dal Zilio, L., Liang, C., & Avouac, J.-P. (2024). Super-shear ruptures steered by pre-stress heterogeneities during the 2023 Kahramanmaraş earthquake doublet. *Nature Communications*, *15*(1), 7004. https://doi.org/10.1038/s41467-024-51446-y

Delph, J., Abgarmi, B., Ward, K. M., Beck, S. L., Özacar, A. A., Zandt, G., et al. (2017). The effects of subduction termination on the continental lithosphere: Linking volcanism, deformation, surface uplift, and slab tearing in central Anatolia. *Geosphere*, *13*(6), 1788–1805. https://doi.org/10.1130/GES01478.1

Delph, J., Darin, M., Whitney, D., Cosca, M., Teyssier, C., Kaymakcı, N., et al. (2024). Deep lithospheric controls on surface deformation and seismicity around the east Anatolian Fault Zone and A3 triple junction. *Geological Society of America Today*, *34*(8), 4–12. https://doi.org/10.1130/GSATG584A.1

Duman, T. Y., & Emre, Ö. (2013). The East Anatolian Fault: Geometry, segmentation and jog characteristics. *Geological Society*, *372*, 495–529. https://doi.org/10.1144/SP372.14

Ergin, M., Aktar, M., & Eyidogan, H. (2004). Present-Day seismicity and seismotectonics of the Cilician Basin: Eastern Mediterranean Region of Turkey. *Bulletin of the Seismological Society of America*, *94*(3), 930–939. https://doi.org/10.1785/0120020153

Ergintav, S., Floyd, M., Paradissis, D., Karabulut, H., Vernant, P., Masson, F., et al. (2023). New geodetic constraints on the role of faults and blocks vs. distribute strain in the Nubia-Arabia-Eurasia zone of active plate interactions. *Turkish Journal of Earth Sciences*, *32*(3), 248–261. https://doi.org/10.55730/1300-0985.1842

Foreman-Mackey, D., Hogg, D. W., Lang, D., & Goodman, J. (2013). Emcee: The MCMC hammer. *Publications of the Astronomical Society of the Pacific*, *125*(925), 306–312. https://doi.org/10.1086/670067

Guidoboni, E., Comastri, A., & Traina, G. (1994). *Catalogue of ancient earthquakes in the Mediterranean area up to the 10th century*. Istituto nazionale di geofisica.

He, L., Feng, G., Xu, W., Wang, Y., Xiong, Z., Gao, H., & Liu, X. (2023). Coseismic kinematics of the 2023 Kahramanmaras, Turkey earthquake sequence from InSAR and optical data. *Geophysical Research Letters*, *50*(17), e2023GL104693. https://doi.org/10.1029/2023GL104693

Herece, E. (2008). *Doğu Anadolu Fayi (DAF) Atlasi, general directorate of mineral research and exploration*. Special Publications. Ser. No. 13.

Jin, Z., & Fialko, Y. (2021). Coseismic and early postseismic deformation due to the 2021 M7.4 Maduo (China) earthquake. *Geophysical Research Letters*, *48*(21), e2021GL095213. https://doi.org/10.1029/2021GL095213

Jia, Z., Jin, Z., Marchandon, M., Ulrich, T., Gabriel, A.-A., Fan, W., et al. (2023). The complex dynamics of the 2023 Kahramanmaraş, Turkey, Mw 7.8-7.7 earthquake doublet. *Science*, *381*(6661), 985–990. https://doi.org/10.1126/science.adi0685

Jin, Z. (2021). Matlab routines for inversion of space geodetic data for subsurface fault slip (Version 2) [Software]. *Zenodo*. https://doi.org/10.5281/zenodo.5528639

Karabulut, H., Güvercin, S. E., Hollingsworth, J., & Konca, A. Ö. (2023). Long silence on the East Anatolian Fault Zone (Southern Turkey) ends with devastating double earthquakes (6 February 2023) over a seismic gap: Implications for the seismic potential in the Eastern Mediterranean region. *Journal of the Geological Society*, *180*(3), jgs2023-021. https://doi.org/10.1144/jgs2023-021

Karabulut, H., Paul, A., Özbakır, A. D., Ergün, T., & Şentürk, S. (2019). A new crustal model of the Anatolia–Aegean domain: Evidence for the dominant role of isostasy in the support of the Anatolian plateau. *Geophysical Journal International*, *218*(1), 57–73. https://doi.org/10.1093/gji/ggz147

Kurt, A. I., Özbakir, A. D., Cingöz, A., Ergintav, S., Doğan, U., & Özarpaci, S. (2023). Contemporary velocity field for Turkey inferred from combination of a dense network of long term GNSS observations. *Turkish Journal of Earth Sciences*, *32*(3), 275–293. https://doi.org/10.55730/1300-0985.1844

Le Pichon, X., & Kreemer, C. (2010). The miocene-to-present kinematic evolution of the Eastern mediterranean and Middle East and its implications for dynamics. *Annual Review of Earth and Planetary Sciences*, *38*(1), 323–351. https://doi.org/10.1146/annurev-earth-040809-152419

Lomax, A. (2023). Precise, NLL-SSST-coherence hypocenter catalog for the 2023 Mw 7.8 and Mw 7.6 SE Turkey earthquake sequence (Version 2) [Dataset]. *Zenodo*. https://doi.org/10.5281/zenodo.7727678

Mahmoud, Y., Masson, F., Meghraoui, M., Cakir, Z., Alchalbi, A., Yavasoglu, H., et al. (2013). Kinematic study at the junction of the East Anatolian fault and the Dead Sea fault from GPS measurements. *Journal of Geodynamics*, *67*, 30–39. https://doi.org/10.1016/j.jog.2012.05.006

McCaffrey, R., Qamar, A. I., King, R. W., Wells, R., Khazaradze, G., Williams, C. A., et al. (2007). Fault locking, block rotation and crustal deformation in the Pacific Northwest. *Geophysical Journal International*, *169*(3), 1315–1340. https://doi.org/10.1111/j.1365-246X.2007.03371.x

McKenzie, D. (1976). The East Anatolian Fault: A major structure in Eastern Turkey. *Earth and Planetary Science Letters*, *29*(1), 189–193. https://doi.org/10.1016/0012-821X(76)90038-8

Nalbant, S. S., McCloskey, J., Steacy, S., & Barka, A. A. (2002). Stress accumulation and increased seismic risk in eastern Turkey. *Earth and Planetary Science Letters*, *195*(3–4), 291–298. https://doi.org/10.1016/S0012-821X(01)00592-1

Özkan, A., Yavaşoğlu, H. H., & Masson, F. (2023). Present-day strain accumulations and fault kinematics at the Hatay Triple Junction using new geodetic constraints. *Tectonophysics*, *854*, 229819. https://doi.org/10.1016/j.tecto.2023.229819

Qu, W., Wang, J., Yang, Y., Gao, Y., Li, J., Wang, Y., et al. (2022). Fine divided method of active tectonic blocks based on adaptive density peak clustering and improved Euler model, revealed by GNSS velocities in Southwest Japan. *Tectonophysics*, *844*, 229635. https://doi.org/10.1016/j.tecto.2022.229635

Reitman, N. G., Briggs, R. W., Barnhart, W. D., Hatem, A. E., Thompson Jobe, J. A., DuRoss, C. B., et al. (2023). Rapid surface rupture mapping from satellite data: The 2023 Kahramanmaraş, Turkey (Türkiye), earthquake sequence. *The Seismic Record*, *3*(4), 289–298. https://doi.org/10.1785/0320230029

Ren, C., Wang, Z., Taymaz, T., Hu, N., Luo, H., Zhao, Z., et al. (2024). Supershear triggering and cascading fault ruptures of the 2023 Kahramanmaraş, Türkiye, Earthquake doublet. *Science*, *383*(6680), 305–311. https://doi.org/10.1126/science.adi1519

Sançar, T., Zabcı, C., Akçar, N., Karabacak, V., Yeşilyurt, S., Yazıcı, M., et al. (2020). Geodynamic importance of the strike-slip faults at the eastern part of the Anatolian Scholle: Inferences from the uplift and slip rate of the Malatya Fault (Malatya-Ovacık Fault Zone, eastern Turkey). *Journal of Asian Earth Sciences*, *188*, 104091. https://doi.org/10.1016/j.jseaes.2019.104091

Savage, J. C. (2018). Euler-Vector clustering of GPS velocities defines microplate geometry in Southwest Japan. *Journal of Geophysical Research: Solid Earth*, *123*(2), 1954–1968. https://doi.org/10.1002/2017JB014874

Savage, J. C., & Burford, R. O. (1973). Geodetic determination of relative plate motion in central California. *Journal of Geophysical Research*, *78*(5), 832–845. https://doi.org/10.1029/JB078i005p00832

Seyitoğlu, G., Tunçel, E., Kaypak, B., Esat, K., & Gökkaya, E. (2022). The Anatolian Diagonal: A broad left lateral shear zone between the North Anatolian Fault Zone and the Aegean/Cyprus Arcs. *Geological Bulletin of Turkey*, *65*, 93–116. https://doi.org/10.25288/tjb.1015537

Shen, Z., Wang, M., Zeng, Y., & Wang, F. (2015). Optimal interpolation of spatially discretized geodetic data. *Bulletin of the Seismological Society of America*, *105*(4), 2117–2127. https://doi.org/10.1785/0120140247

Shimazaki, K., & Nakata, T. (1980). Time-predictable recurrence model for large earthquakes. *Geophysical Research Letters*, *7*(4), 279–282. https://doi.org/10.1029/GL007i004p00279

STL. (2024). Turkey-Earthquake: Emergency Situation Report (05.02.2024). Retrieved from https://reliefweb.int/report/turkiye/turkey-earthquake-emergency-situation-report-05022024

Stucchi, M., Şeşetyan, K., Castelli, V., Gomez Capera, A. A., Meletti, C., & Sbeinati, M. R. (2024). About the "predecessors" of the 2023 February earthquakes, Turkey. *Seismica*, *2*(3). https://doi.org/10.26443/seismica.v2i3.1312

Sun, K. (2025). Interseismic GNSS velocity field in SE Türkiye and Coseismic deformation fields (InSAR, POT, and GNSS) of the 2023 Türkiye earthquake doublet (Version 1) [Dataset]. *Zenodo*. https://doi.org/10.5281/zenodo.17113589

Tan, O. (2021). A homogeneous earthquake catalogue for Turkey. *Natural Hazards and Earth System Sciences*, *21*(7), 2059–2073. https://doi.org/10.5194/nhess-21-2059-2021

Tan, O., Tapirdamaz, M. C., & Yörük, A. (2008). The earthquake catalogues for Turkey. *Turkish Journal of Earth Sciences*, *17*, 405–418.

Vavra, E., Fialko, Y., Bulut, F., Garagon, A., Yalvaç, S., & Yaltırak, C. (2025). The 2023 Mw 7.8–7.7 Kahramanmaraş earthquakes were loosely slip-predictable. *Communications Earth and Environment*, *6*(1), 80. https://doi.org/10.1038/s43247-024-01969-5

Walters, R. J., Parsons, B., & Wright, T. J. (2014). Constraining crustal velocity fields with InSAR for Eastern Turkey: Limits to the block-like behavior of Eastern Anatolia. *Journal of Geophysical Research: Solid Earth*, *119*(6), 5215–5234. https://doi.org/10.1002/2013JB010909

Weertman, J., & Weertman, J. R. (1964). In *Elementary dislocation theory* (p. 213). Macmillan.

Weiss, J. R., Walters, R. J., Morishita, Y., Wright, T. J., Lazecky, M., Wang, H., et al. (2020). High-Resolution surface velocities and strain for Anatolia from Sentinel-1 InSAR and GNSS data. *Geophysical Research Letters*, *47*(17), e2020GL087376. https://doi.org/10.1029/2020GL087376

Wessel, P., Luis, J. F., Uieda, L., Scharroo, R., Wobbe, F., Smith, W. H. F., & Tian, D. (2019). The generic mapping tools version 6. *Geochemistry, Geophysics, Geosystems*, *20*(11), 5556–5564. https://doi.org/10.1029/2019GC008515

Xu, R., & Stamps, D. S. (2019). Strain accommodation in the Daliangshan Mountain area, Southeastern Margin of the Tibetan Plateau. *Journal of Geophysical Research: Solid Earth*, *124*(9), 9816–9832. https://doi.org/10.1029/2019JB017614

Yönlü, Ö., Altunel, E., & Karabacak, V. (2017). Geological and geomorphological evidence for the southwestern extension of the East Anatolian Fault Zone, Turkey. *Earth and Planetary Science Letters*, *469*, 1–14. https://doi.org/10.1016/j.epsl.2017.03.034

Zelenin, E., Bachmanov, D., Garipova, S., Trifonov, V., & Kozhurin, A. (2022). The Active Faults of Eurasia Database (AFEAD): The ontology and design behind the continental-scale dataset. *Earth System Science Data*, *14*(10), 4489–4503. https://doi.org/10.5194/essd-14-4489-2022

References From the Supporting Information

Barbot, S., Luo, H., Wang, T., Hamiel, Y., Piatibratova, O., Javed, M. T., et al. (2023). Slip distribution of the February 6, 2023 Mw 7.8 and Mw 7.6, Kahramanmaraş, Turkey earthquake sequence in the East Anatolian Fault Zone. *Seismica*, *2*(3). https://doi.org/10.26443/seismica.v2i3.502

Basili, R., Kastelic, V., Demircioglu Tumsa, M. B., Garcia Moreno, D., Nemser, E. S., Petricca, P., et al. (2013). The European Database of Seismogenic Faults (EDSF) compiled in the framework of the Project SHARE. *Data set]*. https://doi.org/10.6092/INGV.IT-SHARE-EDSF

Cavalié, O., & Jónsson, S. (2014). Block-like plate movements in eastern Anatolia observed by InSAR. *Geophysical Research Letters*, *41*(1), 26–31. https://doi.org/10.1002/2013GL058170

Costantini, M. (1998). A novel phase unwrapping method based on network programming. *IEEE Transactions on Geoscience and Remote Sensing*, *36*(3), 813–821. https://doi.org/10.1109/36.673674

Davies, D. L., & Bouldin, D. W. (1979). A cluster separation measure. *IEEE Transactions on Pattern Analysis and Machine Intelligence*, *PAMI-1*(2), 224–227. https://doi.org/10.1109/TPAMI.1979.4766909

Emre, Ö., Duman, T., Özalp, S., Elmaci, H., Olgun, Ş., & Şaroğlu, F. (2013). *Active fault map of Turkey with an explanatory text. 1:1,250,000 Scale*. General Directorate of Mineral Research and Exploration.

Goldstein, R. M., & Werner, C. L. (1998). Radar interferogram filtering for geophysical applications. *Geophysical Research Letters*, *25*(21), 4035–4038. https://doi.org/10.1029/1998GL900033

Güvercin, S. E., Karabulut, H., Konca, A. Ö., Doğan, U., & Ergintav, S. (2022). Active seismotectonics of the East Anatolian Fault. *Geophysical Journal International*, *230*(1), 50–69. https://doi.org/10.1093/gji/ggac045

Liu, C., Lay, T., Wang, R., Taymaz, T., Xie, Z., Xiong, X., et al. (2023). Complex multi-fault rupture and triggering during the 2023 earthquake doublet in southeastern Türkiye. *Nature Communications*, *14*(1), 5564. https://doi.org/10.1038/s41467-023-41404-5

Ma, Z., Li, C., Jiang, Y., Chen, Y., Yin, X., Aoki, Y., et al. (2024). Space geodetic insights to the dramatic stress rotation induced by the February 2023 Turkey-Syria earthquake doublet. *Geophysical Research Letters*, *51*(6), e2023GL107788. https://doi.org/10.1029/2023GL107788

Purnima Bholowalia, A. K. (2014). EBK-Means: A clustering technique based on elbow method and K-Means in WSN. *International Journal of Computer Applications*, *105*(9), 17–24. https://doi.org/10.5120/18405-9674

Reilinger, R. E., McClusky, S. C., Vernant, P., Lawrence, S., Ergintav, S., Cakmak, R., et al. (2006). GPS constraints on continental deformation in the Africa-Arabia-Eurasia continental collision zone and implications for the dynamics of plate interactions. *Journal of Geophysical Research*, *111*(B5), 2005JB004051. https://doi.org/10.1029/2005JB004051

Rousseeuw, P. J. (1987). Silhouettes: A graphical aid to the interpretation and validation of cluster analysis. *Journal of Computational and Applied Mathematics*, *20*, 53–65. https://doi.org/10.1016/0377-0427(87)90125-7

Sunbul, F. (2019). Time-dependent stress increase along the major faults in eastern Turkey. *Journal of Geodynamics*, *126*, 23–31. https://doi.org/10.1016/j.jog.2019.03.001

Tibshirani, R., Walther, G., & Hastie, T. (2001). Estimating the number of clusters in a data set via the gap statistic. *Journal of the Royal Statistical Society: Series B*, *63*(2), 411–423. https://doi.org/10.1111/1467-9868.00293

Wang, K., Xu, X., & Hu, Y. (2024). Kinematics of the 2023 Kahramanmaraş earthquake doublet: Biased near-fault data and shallow slip deficit. *Seismological Research Letters*, *96*(2A), 828–837. https://doi.org/10.1785/0220240062

Wang, K., & Fialko, Y. (2014). Space geodetic observations and models of postseismic deformation due to the 2005 M7.6 Kashmir (Pakistan) earthquake. *Journal of Geophysical Research: Solid Earth*, *119*(9), 7306–7318. https://doi.org/10.1002/2014JB011122

Xu, L., Mohanna, S., Meng, L., Ji, C., Ampuero, J.-P., Yunjun, Z., et al. (2023). The overall-subshear and multi-segment rupture of the 2023 Mw 7.8 Kahramanmaraş, Turkey earthquake in millennia supercycle. *Communications Earth and Environment*, *4*(1), 379. https://doi.org/10.1038/s43247-023-01030-x